A Modeling Study of a Low-Level Jet along the Yun-Gui Plateau in South China

MING-YANG HE

State Key Laboratory of Numerical Modeling for Atmospheric Sciences and Geophysical Fluid Dynamics, Institute of Atmospheric Physics, Chinese Academy of Sciences, and University of Chinese Academy of Sciences, Beijing, China

HONG-BO LIU

State Key Laboratory of Numerical Modeling for Atmospheric Sciences and Geophysical Fluid Dynamics, Institute of Atmospheric Physics, Chinese Academy of Sciences, Beijing, China

BIN WANG

State Key Laboratory of Numerical Modeling for Atmospheric Sciences and Geophysical Fluid Dynamics, Institute of Atmospheric Physics, Chinese Academy of Sciences, and Center for Earth System Science, Tsinghua University, Beijing, China

DA-LIN ZHANG

Department of Atmospheric and Oceanic Science, University of Maryland, College Park, College Park, Maryland

(Manuscript received 4 March 2015, in final form 30 July 2015)

ABSTRACT

In this study, the three-dimensional structures and diurnal evolution of a typical low-level jet (LLJ) with a maximum speed of 24 m s^{-1} occurring in the 850–800-hPa layer are examined using both large-scale analysis and a high-resolution model simulation. The LLJ occurred on the eastern foothills of the Yun-Gui Plateau in south China from 1400 LST 29 June to 1400 LST 30 June 2003. The effects of surface radiative heating, topography, and latent heat release on the development of the LLJ case are also studied. Results show that a western Pacific Ocean subtropical high and a low pressure system on the respective southeast and northwest sides of the LLJ provide a favorable large-scale mean pressure pattern for the LLJ development. The LLJ reaches its peak intensity at 850 hPa near 0200 LST with wind directions veering from southerly before sunset to southwesterly at midnight. A hodograph at the LLJ core shows a complete diurnal cycle of the horizontal wind with a radius of 5.5 m s^{-1}. It is found that in an LLJ coordinates system the along-LLJ geostrophic component regulates the distribution and 65% of the intensity of LLJ, whereas the ageostrophic component contributes to the clockwise rotation, thus leading to the formation and weakening of the LLJ during night- and daytime, respectively. Numerical sensitivity experiments confirm the surface radiative heating as the key factor in determining the formation of the nocturnal LLJ. The existence of the Yun-Gui Plateau, and the downstream condensational heating along the mei-yu front play secondary roles in the LLJ formation.

1. Introduction

The low-level jet (LLJ), typically referred to as a fast-moving airflow in the lowest kilometers, has been found at many locations around the world, such as North America, South America, southeast China, South Africa, the Indian subcontinent, Australia, and Antarctica (Stensrud 1996; Muñoz and Garreaud 2005; Rife et al. 2010; Du et al. 2014). LLJs tend to develop over the eastern slope of large mountains or coastal regions having significant land–sea temperature contrasts, with the wind directions usually parallel to the mountain orientations or coastline (Ardanuy 1979; Douglas 1995; Zhang et al. 2006; Du et al. 2015a,b). The subject of LLJs has drawn considerable attention since the 1930s (Goualt 1938; Farquharson 1939) not only because of the interesting aspects of the phenomena, but also because of their influence on weather

Denotes Open Access content.

Corresponding author address: Dr. Hong-Bo Liu, LASG, Institute of Atmospheric Physics, Chinese Academy of Sciences, Beijing 100029, China.
E-mail: hongboliu@mail.iap.ac.cn

DOI: 10.1175/JAMC-D-15-0067.1

and regional climate (Stensrud 1996; Zhang et al. 2006). An LLJ can provide a favorable environment with an ample supply of water vapor for the occurrence of heavy rainfall (Maddox 1980; Tao 1980; Zhang and Fritsch 1986; Arritt et al. 1997; Higgins et al. 1997; Qian et al. 2004). In addition, the relationships between LLJs and air pollution, wind energy, aviation safety, forest fires, as well as bird migration have become the focus of interdisciplinary research in the recent two decades (Liechti and Schaller 1999; Taubman et al. 2004; Archer and Jacobson 2005; Storm et al. 2008).

Despite considerable research being done in LLJ studies, little is yet known about the characteristics and variability of LLJs over the mountainous regions of south China, especially over the complex terrain along the east of the Tibetan Plateau, as a result of the lack of high-resolution observations. It is encouraging that some recent modeling studies have examined the spatial and diurnal variations of LLJs in China (e.g., Du et al. 2014). So far, most of the previous studies focused on the relationship between LLJs and heavy rainfall, especially the mei-yu frontal rainfall (e.g., Sun and Zhai 1980; Zhao and Zhou 2001; Wang et al. 2003). The mei-yu fronts are often distributed in the middle to lower reaches of the Yangtze River basin during every June and July, and they are characterized by weak temperature gradients but high equivalent potential temperature θ_e gradients due to strong meridional moisture contrasts and by large horizontal wind shear. The quasi-steady mei-yu frontal systems often generate heavy rainfall (Ding 1994; Liu et al. 2008). Qian et al. (2004) demonstrated that mesoscale circulation patterns resulting from mei-yu frontal condensational heating act to increase the maximum wind speed of an LLJ and, therefore, strengthen the moisture transport for the generation of heavy rainfall. However, the LLJs they discussed (and in some other studies) only involved a narrow zone of high-speed airflow at a low level without considering a jetlike vertical wind profile and its possible diurnal variations. Such a flow regime has been defined by Stensrud (1996) as a low-level jet stream, which may be generated by different processes from an LLJ. These regimes may produce different influences on the development of mesoscale convective systems (MCSs) in the absence of vertical wind shear aloft. In this regard, Du et al. (2012) showed a synoptic-scale LLJ stream that differed from the LLJ associated with the planetary boundary layer (PBL).

Inertial oscillation theory, first proposed by Blackadar (1957) and recently supplemented by Van de Wiel et al. (2010), appears to be robust for explaining the formation of typical LLJs in the PBL over a plain region. Holton (1967) emphasized the effects of thermal forcing on the diurnal oscillation of the PBL winds above sloping terrain. Bonner and Paegle (1970) clarified the theory of Holton (1967) in a more simplified and physical way. The air near the surface over the high terrain is warmer (cooler) than the air above the surface over lower terrain after sunrise (sunset). The diurnal oscillation of the horizontal temperature gradient can lead to the reversal of thermal winds, and then enhance or decrease the magnitude of horizontal winds near the top of the PBL. Recently, Du and Rotunno (2014) demonstrated with a simple one-dimensional model that both Blackadar's and Holton's mechanisms are important for the formation of LLJs over the Great Plains of the United States.

Using 2-yr wind profiler data and model simulation results, Zhang et al. (2006) found that the LLJs tend to be peaked in the middle portion of the sloping terrain, following closely the orientation of the Appalachians Mountains. They selected a typical LLJ case to examine its formation mechanisms, which developed under the influence of a subtropical high with little convective activity. Sensitivity simulations show that eliminating the surface heat flux produces the most significant impact on the development of the LLJ, and orography tends to enhance the intensity of the LLJ and elevate its altitude. The previous studies suggest clearly that the dynamic and thermodynamic forcings by different terrain profiles, land surface characteristics, and synoptic conditions, as well as diabatic heating, could all contribute to the formation of LLJs. However, our understanding of their relative contributions is far from perfect.

Based on the sensitivity simulations of reducing 50% of mountain heights, Sun and Lorenzo (1985) claimed that the Tibetan Plateau is responsible for the formation of LLJs in south China. This result is similar to the impact of the Rocky Mountains on LLJs in North America and the highlands of East Africa on the Somalia LLJ. However, unlike North and South America, East Asia can be characterized by "three stair steps" of topography from the west to east: the Tibetan Plateau (25°–40°N, 70°–105°E) at 4000–5000 m, the Yun-Gui Plateau (20°–30°N, 95°–115°E) at 2000–2500 m including most territories of Yunnan and Guizhou Provinces, and the southeastern mountains of lower than 1000 m (20°–30°N, 105°–122°E), plus the plain regions in east China (see Fig. 1). Few of the previous studies have distinguished their different influences on the ambient flows but instead handled them as a whole (Liu and Jiao 2000). In reality, these complicated terrain features must produce nonlinear influences on the development of LLJs and MCSs (Zhao 2012). Thus, it is highly desirable to examine the roles of the three stair steps terrain in the development of LLJs over south China.

In this study, a typical LLJ event with a maximum speed of 24 m s^{-1} occurring over the eastern sloping terrain in south China during a 24-h period from 1400 LST (0600 UTC) 29 June to 1400 LST (0600 UTC) 30 June

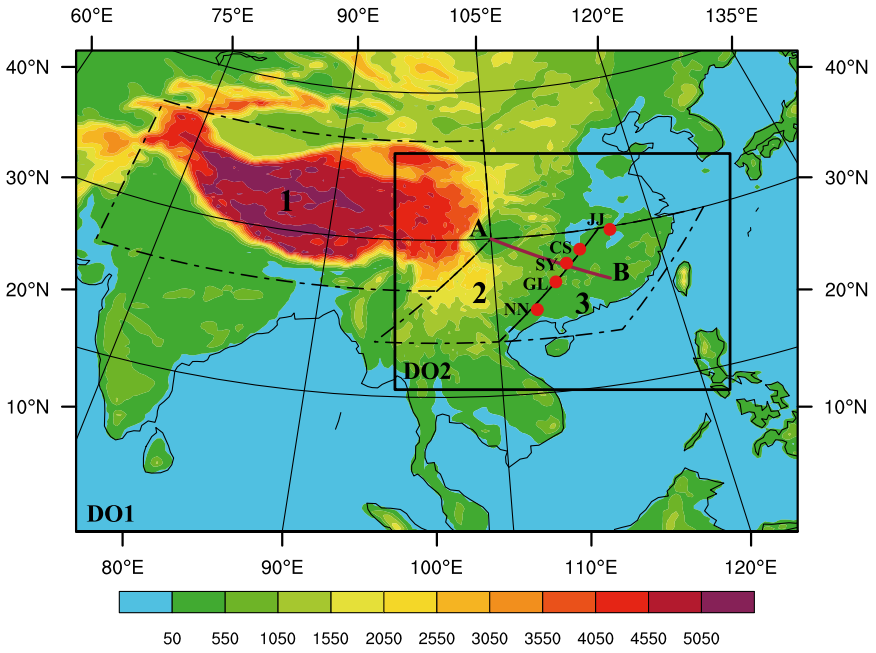

FIG. 1. The double-nested model grid domains with topography at intervals of 500 m (shaded). Letters JJ, CS, SY, GL, and NN denote the stations defined in the text. Numbers 1, 2, and 3 denote the Tibetan Plateau, Yun-Gui Plateau, and southeastern mountains. Line A–B is used for cross sections shown in Fig. 4.

2003 is examined (Liu et al. 2012). This event occurred under favorable large-scale synoptic conditions, namely, with a subtropical high and a low pressure system on the southeast and northwest sides of the LLJ, respectively. Therefore, it provides a representative case for examining the roles of various factors in the formation of the LLJ. In addition, heavy rainfall occurred at the exit region of the LLJ, which was 400–500 km away from the LLJ core, making it possible to minimize the effects of diabatic heating. Thus, the objectives of this study are to (i) examine the three-dimensional structures and evolution of the LLJ over the eastern foothills of the Yun-Gui Plateau and (ii) isolate the impacts of different parameters on the development of the LLJ, especially synoptic forcing, surface radiative heating, and topography by using a series of sensitivity simulations.

The next section provides model description and verification. The large-scale aspects of the LLJs from both the observations and simulation will be presented. Section 3 shows the diurnal variations of the LLJ and its geostrophic and ageostrophic components from the model simulation. The unbalanced aspect of the LLJ will also be examined by calculating the horizontal momentum budget in an LLJ coordinates system. Section 4 examines the sensitivity of the model-simulated LLJ to surface heating, topography, and diabatic heating. A summary and concluding remarks are given in the final section.

2. Model description and verification

a. Model description

A two-way interactive, doubly nested grid (36 and 12 km), nonhydrostatic version 3.4 of the Weather Research and Forecasting Model (WRF; Skamarock et al. 2008) is used to simulate the LLJ event and analyze its characteristics and evolution. Figure 1 shows the nested domains with the coarse-mesh domain covering most of Asia and the northwestern Pacific, and the fine-mesh domain including the southeastern portion of China. Note that the fine-mesh domain covers the three stair steps of complex terrain in south China, as mentioned earlier. There are 33 levels (i.e., 32 layers) in the vertical (η = 1.0, 0.993, 0.983, 0.97, 0.954, 0.934, 0.909, 0.88, 0.837, 0.795, 0.752, 0.71, 0.635, 0.566, 0.503, 0.445, 0.392, 0.344, 0.3, 0.26, 0.223, 0.19, 0.16, 0.133, 0.109, 0.087, 0.069, 0.053, 0.039, 0.027, 0.017, 0.007, and 0), with η = 1.0 corresponding to the bottom boundary. The model top is set at 50 hPa.

The model water cycles used for this study include (i) the Ferrier (new Eta) microphysics scheme with diagnostic mixed-phase processes (Rogers et al. 2001; Ferrier et al. 2002), (ii) the Kain–Fritsch convective parameterization scheme including the effects of shallow convection (Kain 2004), (iii) the level-2.5 turbulent kinetic energy PBL scheme (Nakanishi and Niino 2006), (iv) a Rapid Radiative Transfer Model for longwave and Dudhia's (1989)

scheme for shortwave radiation parameterizations, and (v) the Noah land surface model (Chen and Dudhia 2001).

The model initial and lateral boundary conditions are taken from the NCEP Final (FNL) operational global analysis at 1.0° grid resolution and 6-hourly intervals (online at http://dss.ucar.edu/datasets/ds083.2/), with nine levels below 700 hPa. The sea surface temperature (SST) field is obtained by linearly interpolating in both time (from daily to 6 hourly) and space from the NCEP Marine Modeling and Analysis Branch Real Time Global (RTG) daily SST dataset at 0.5° resolution (Thiébaux et al. 2003; http://polar.ncep.noaa.gov/sst/rtg_low_res/). To capture the structures and evolution of the LLJ event and the associated rainfall, all of the numerical simulations are initialized at 0800 LST (0000 UTC) 29 June and then integrated for 30 h, valid at 1400 LST (0600 UTC) 30 June 2003. The first 6-h integrations are treated as the model spinup period, so they are not used for the model analysis. Both the outermost lateral boundary conditions and SST are updated every 6 h, and the hourly model output is used to analyze the diurnal variations of the LLJ.

It should be mentioned that despite the coarse spatial and temporal resolutions, horizontal winds do exhibit vertical jetlike profiles in both the twice-daily conventional soundings and 6-hourly FNL analysis, especially at 0800 LST 30 June 2003 (not shown). Therefore, we may use the FNL analysis to validate the model-simulated flow fields to be presented in the next subsection.

b. *Model verification and large-scale aspects of the LLJ*

Figure 2a shows the distribution of horizontal winds at 850 hPa from the NCEP FNL analysis at 0200 LST 30 June 2003, when the LLJ under study reached its maximum intensity of more than 20 m s^{-1} in Hunan Province (centered at 27°N, 112°E). A large portion of south China was covered with an intense warm and moist airstream of more than 12 m s^{-1}, whose axis extended from the southwest coast northeastward to the East China Sea. Of particular relevance to this study is that the major portion of the LLJ followed closely the orientation of the Yun-Gui Plateau (i.e., between regions 2 and 3 in Fig. 1; cf. Figs. 2a and 1), and it was located in the northwestern portion of the western Pacific subtropical high (WPSH), as shown by the 500-hPa 5880-m geopotential height contour. During the period of 28–30 June, the WPSH extended northwestward and strengthened with the 5880-m height contour displacing from east of Taiwan Island to China's southeastern coast (not shown). This northwestward displacement provided a more favorable set of background conditions for the formation of the LLJ as a result of the increased northwestward pressure gradient force associated with the WPSH and the southwest vortex over the

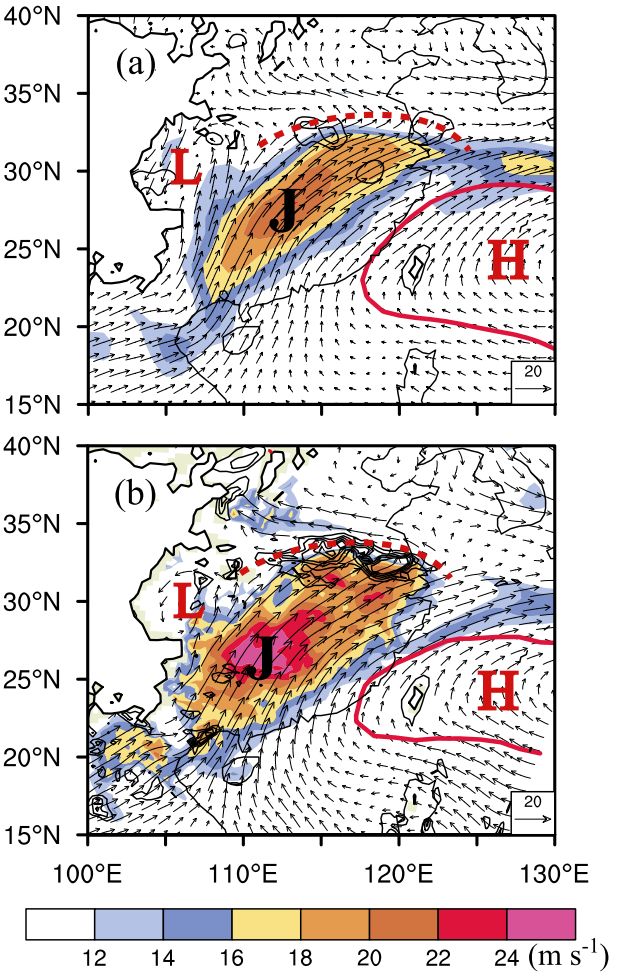

FIG. 2. Distribution of horizontal wind vectors and speeds (shaded, m s^{-1}) at 850 hPa from (a) the NCEP FNL analysis and (b) the WRF simulation. Superimposed is the 6-houly accumulated rainfall (contoured at intervals of 8 mm) from 706 hourly rain gauge stations at roughly 1.0° resolution in east China in (a), which have been subjected to critical quality control (Yu et al. 2007), and the WRF simulation in (b), valid at 0200 LST 30 Jun 2003. The solid line and dotted lines in red refer to the 5880-m geopotential isoline at 500 hPa and the wind shear line at 850 hPa, respectively. Letters J, L, and H mark the location of the LLJ core and the centers of a southwest vortex and subtropical high, respectively. The blank area in the northwest portion of the domain denotes the distribution of 1500-m terrain elevation. Similar conventions apply for the following figures.

Sichuan basin, as will be further shown in the next section. The southwesterly LLJ brought ample water vapor from tropical oceans that was then converged along a narrow belt of extremely weak winds near 33°N, where a mei-yu front was located. As a result, heavy rainfall occurred on the cyclonic-side, exit region of the LLJ.

In general, the horizontal distribution and intensity of the large-scale circulation system, and the LLJ, as well as rainfall, are all well captured by the WRF Model throughout the simulation period. The only major exception is that

the simulated LLJ core is about 100 km to the west of that in the analysis (cf. Figs. 2a and 2b). Since this 100-km difference is close to the horizontal resolution of the analysis, we may claim that the WRF simulates well the general horizontal structure and coverage of the LLJ. The model simulation shows that the low-level southwesterly winds began to increase in strength and area coverage after sunset, except for the northern part that did not follow the terrain orientation (i.e., the Taihang Mountains) in northern China but veered eastward to the East China Sea. This flow regime may be attributed partly to the influences of southwesterly monsoonal flows and the presence of the WPSH (Ding et al. 2007), and partly to the distribution of the mei-yu front as well as diabatic heating along the mei-yu front (Qian et al. 2004). Both the observed and the simulated LLJs had a width of 700–800 km and a length scale of more than 1600 km. The horizontal wind speed had an 8–10 m s^{-1} sharp decrease from the core region to the edge within a 400-km belt (Figs. 2a,b).

In the vertical, the LLJ cores of more than 20 m s^{-1} from both the analysis and simulation were located mostly in the 850–800-hPa layer with significant decreases in wind speed above (Figs. 3 and 4), so they were indeed LLJs as typically defined rather than LLJ streams. To further explore these features, vertical wind profiles at five stations (i.e., along the LLJ axis) are selected to analyze the vertical characteristics of the LLJs, which are Nanning (NN), Guilin (GL), Shaoyang (SY), Changsha (CS), and Jiujiang (JJ), as dotted in Fig. 1, with station elevations of 72, 162, 249, 45, and 32 m, respectively. On average, the altitudes of the maximum wind speeds in the NCEP FNL analysis (and upward decreases) were somewhat higher (smaller) than those simulated by the WRF (cf. Figs. 3a and 3b). That is, the LLJs at NN, GL, SY, CS, and JJ were peaked at 850 (900), 800 (825), 800 (850), 850 (850), and 850 (925) hPa from the analysis (WRF simulation). Although the LLJs are strong, more than 17 m s^{-1} at their peak times, the wind speeds decrease more slowly upward than downward from the core level at these stations. The presence of strong wind speeds above the LLJ core level is consistent with the large-scale mean pressure pattern (i.e., with a subtropical high and a distinct low pressure system on the southeast and northwest, respectively; see Fig. 2).

Figure 4a shows the vertical cross-sectional structures of the LLJ along line A–B (see Fig. 1) over south China from the analysis. There was a distinct local wind maximum of larger than 22 m s^{-1} near 800 hPa that decreases rapidly upward. The relative location of the LLJ to the Yun-Gui Plateau was similar in characteristics to that of the LLJ to the Rocky Mountains in North America (Weaver and Nigam 2008). By comparison, the simulated LLJ exhibits more detailed structures in relation to higher-resolution topography (Fig. 4b). The LLJ occurs along the northeastern foothills of the Yun-Gui Plateau; its relative position is similar to that presented by Zhang et al. (2006) in association with the Appalachian Mountains. In particular, the WRF appears not only to capture well the LLJ core in the analysis, but also to extend its fast speed down to 900 hPa, thus generating a

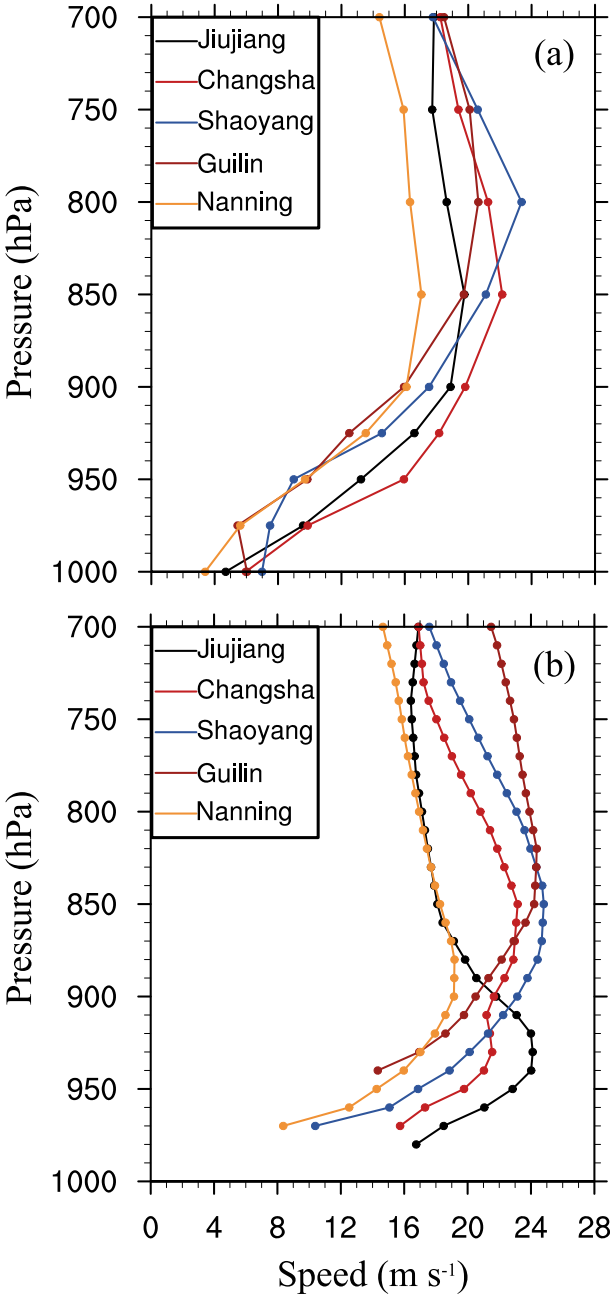

FIG. 3. Vertical profiles of horizontal wind speeds (m s^{-1}) from (a) the NCEP FNL analysis and (b) the WRF simulation at JJ (black), CS (red), SY (blue), GL (brown), and NN (orange), valid at 0200 LST 30 Jun 2003. See Fig. 1 for their locations.

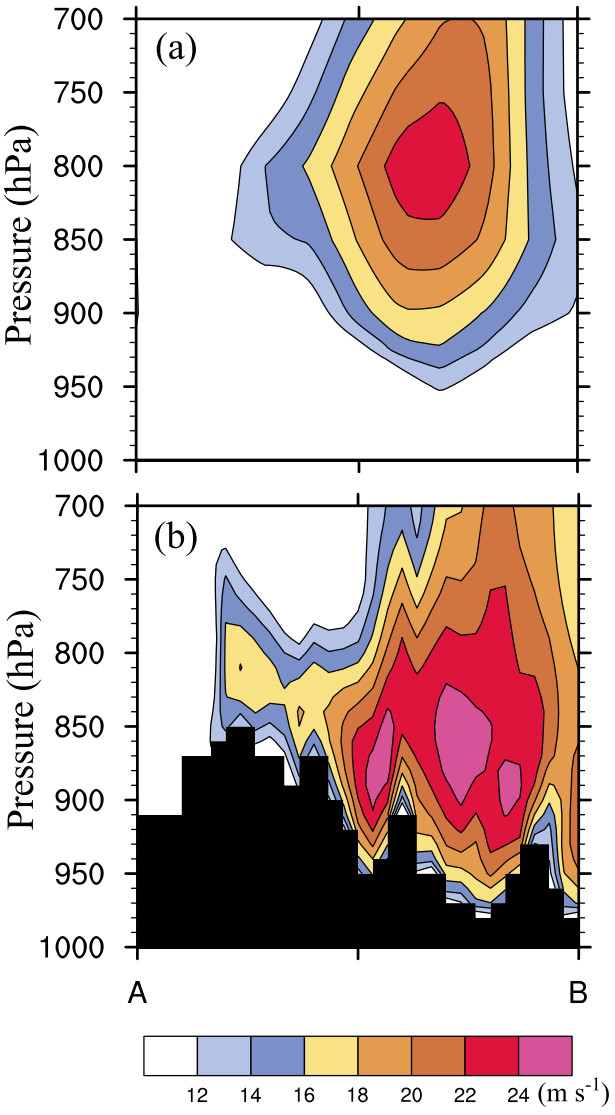

FIG. 4. Vertical cross section of horizontal wind speeds (shaded, m s^{-1}) along line A–B in Fig. 1, which is taken normal to the LLJ axis and through the LLJ core, from (a) the NCEP FNL analysis and (b) the WRF simulation, valid at 0200 LST 30 Jun 2003. Wind speeds larger than 12 m s^{-1} are contoured at intervals of 2 m s^{-1}. Black-shaded areas in (b) indicate the distribution of the WRF model terrain.

larger volume of fast currents centered at 850 hPa. Given the sensitivity of the LLJ core height to terrain heights and the presence of different terrain heights between the FNL analysis and WRF simulation, we may consider the WRF-simulated LLJ structures to offer a reasonable representation of the observed environment. With the above model verifications, we may state that the WRF simulation provides sufficient credibility for analyzing the LLJ characteristics in the next two sections that could not be revealed by the analysis data because of its coarse spatial and temporal resolutions.

3. Diurnal characteristics of the LLJ

a. Diurnal variation

Figures 5a and 5c show the hourly time series of the WRF-simulated horizontal wind profiles, together with the associated hodograph at 850 hPa, at the SY station where the LLJ core is located. We see a clear diurnal variation of the low-level wind field with the LLJ occurring after midnight (Fig. 5a). That is, the horizontal wind below 850 hPa is less than 16 m s^{-1} before sunset, and neither the wind speeds nor directions vary much in the PBL as a result of vertical turbulence mixing. Wind speeds begin to accelerate near 2000 LST when they are decoupled from the surface friction, and such acceleration is more obvious in the 950–800-hPa layer (Fig. 5a). Meanwhile, wind directions below 800 hPa veer from southerly before sunset to southwesterly during nighttime (Fig. 5c) as a result of the inertial oscillation of ageostrophic winds. Wind speeds reach their peak intensity of greater than 24 m s^{-1} at 850 hPa near 0200 LST. The LLJ maintains its high intensity until 0600 LST 30 June and then decreases gradually as the second daytime cycle begins. The temporal evolution and clockwise rotation of the horizontal velocity at 850 hPa could be clearly seen from the elongated hodograph in Fig. 5c covering a complete diurnal cycle of the horizontal wind at the LLJ core. Without the passage of a new weather system, the above diurnal cycle repeats on the next day (not shown).

To better quantify the relative contributions of various factors to the development of the LLJ and illustrate the associated temporal characteristics, an LLJ coordinates system is adopted, based on the hodograph shown in Fig. 5c. In the LLJ coordinates, the s axis is defined by averaging 24-h wind directions in the LLJ core while the n axis is just perpendicular to the s axis and directed to the right (Fig. 5b), just like the rotated Cartesian (x, y) coordinates. In the LLJ coordinates, both the along V_s and normal V_n components of the horizontal wind at the core region have a diurnal variation of about 11 m s^{-1} (i.e., between 14 and 25 m s^{-1} for V_s, and between −6 and 5 m s^{-1} for V_n) during the 24-h period, even though the hodograph is elongated. This is consistent with the inertial oscillation theory of Blackadar (1957).

We find that the vertical profiles of horizontal winds and hodographs at the other four stations (i.e., JJ, CS, GL, and NN) show similar temporal characteristics as those at the SY station, although they differ in their magnitude and timing of peak wind speed, the altitude of the LLJ core, and the size of the inertial circle (Fig. 6). Among the five stations, the LLJ is strongest (>24 m s^{-1}) at SY and weakest (~20 m s^{-1}) at NN. Overall, the timing of peak wind speed appears earlier at stations in the south

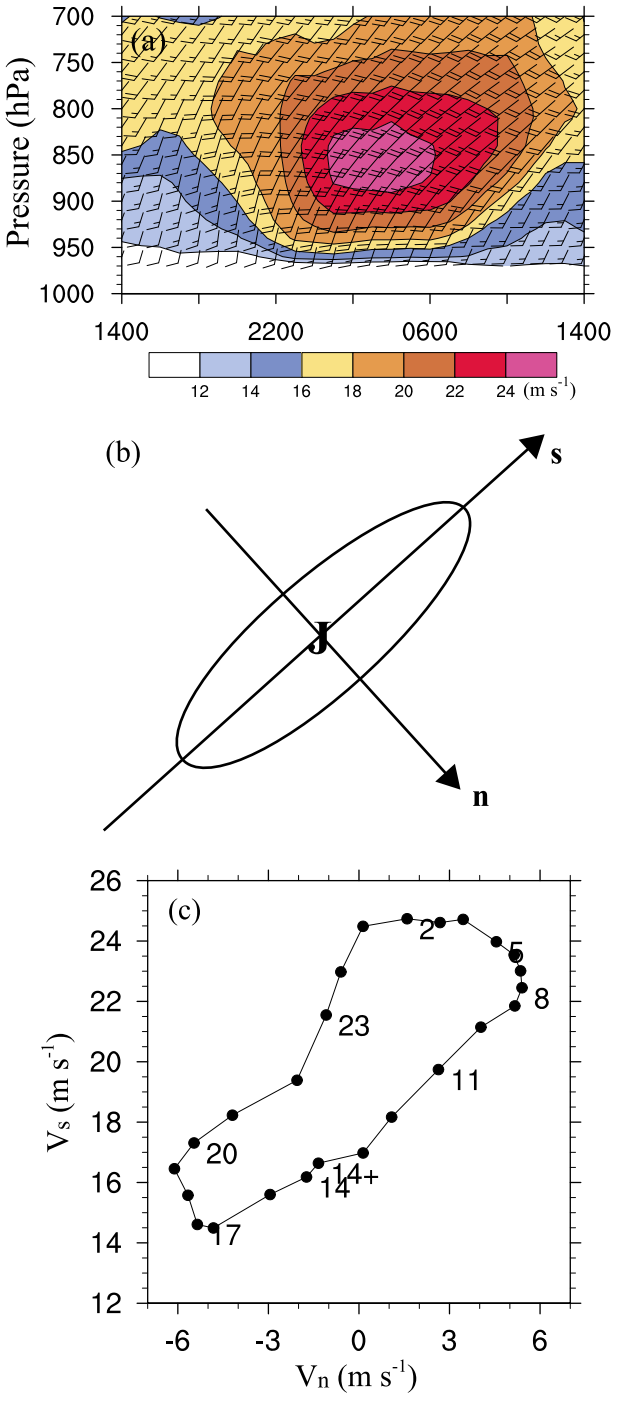

FIG. 5. (a) Time–height cross section of horizontal wind speeds (shaded, m s^{-1}) and wind barbs (a full barb is 10 m s^{-1}) with the speed larger than 12 m s^{-1} contoured at intervals of 2 m s^{-1}, (b) a schematic diagram of the LLJ coordinates, and (c) a hodograph at hourly intervals taken at 850 hPa at SY from the WRF simulation during the period 1400 LST 29 Jun–1400 LST 30 Jun 2003.

(e.g., GL and NN) and later in the north (e.g., CS). However, the size of the inertial circles decreases from north to south (e.g., from ~6.0 m s^{-1} at JJ to ~2.5 m s^{-1} at NN), as dictated partly by the local Coriolis parameter. Therefore, we may state that the effect of inertial oscillation is less important at stations GL and NN than those at the other three stations. This further suggests that inertial oscillation theory is applicable to the formation of the present LLJ event, at least, partly.

Figure 7 shows the horizontal distribution of deviation wind vectors from the 24-h average at 850 hPa at five typical phases of the LLJ diurnal cycle (i.e., 1400 and 2000 LST 29 June and 0200, 0800, and 1400 LST 30 June 2003). The clockwise rotation of the low-level deviation wind vectors in east China is obvious. The deviation wind vectors in the LLJ core region exhibit nearly 90° directional shifts every 6 h as part of the inertial oscillation (i.e., from northeasterly to southeasterly, southwesterly, and northwesterly between 1400 LST 29 June and 0800 LST 30 June; see Figs. 7a–d). The northeasterly and southwesterly deviation winds correspond to the weakest and strongest LLJs at 1400 LST 29 June and 0200 LST 30 June (cf. Figs. 5 and 7a,c), respectively. The strongest and weakest intensity phases appear to be attributable partly to the variation of synoptic forcing, and partly to the diurnal heating cycle associated with the sloping topography (i.e., the Yun-Gui Plateau versus lower mountains and plains to the east). This will be further examined in the next section.

In view of the existence of pronounced background flows in the present case, it is desirable to determine the contributions of large-scale motion versus various local forcings to the formation of the LLJ. Thus, in the next subsections, we separate the geostrophic and ageostrophic components of the LLJ to isolate the large-scale contributions, and then perform horizontal momentum budget calculations to examine unbalanced characteristics of the LLJ.

b. Geostrophic versus ageostrophic components of the LLJ

Figures 8 and 9 show the horizontal distribution of the respective geostrophic $\mathbf{V}_g$ and ageostrophic $\mathbf{V}_{ag}$ components of the horizontal winds at 850 hPa at 6-hourly intervals. Although both $\mathbf{V}_g$ and $\mathbf{V}_{ag}$ show some wavelike characteristics, southwesterly $\mathbf{V}_g$ dominates east China, with the core region located 1°–2° to the south of the LLJ core (Figs. 8a–c). As the WPSH extends northwestward, the increased northwest–southeastward pressure gradient results in the strengthening of $\mathbf{V}_g$ from 1400 LST 29 June to 0800 LST 30 June, while exhibiting small directional shifts throughout the 24-h period. By comparison, the $\mathbf{V}_{ag}$ field shows quite different

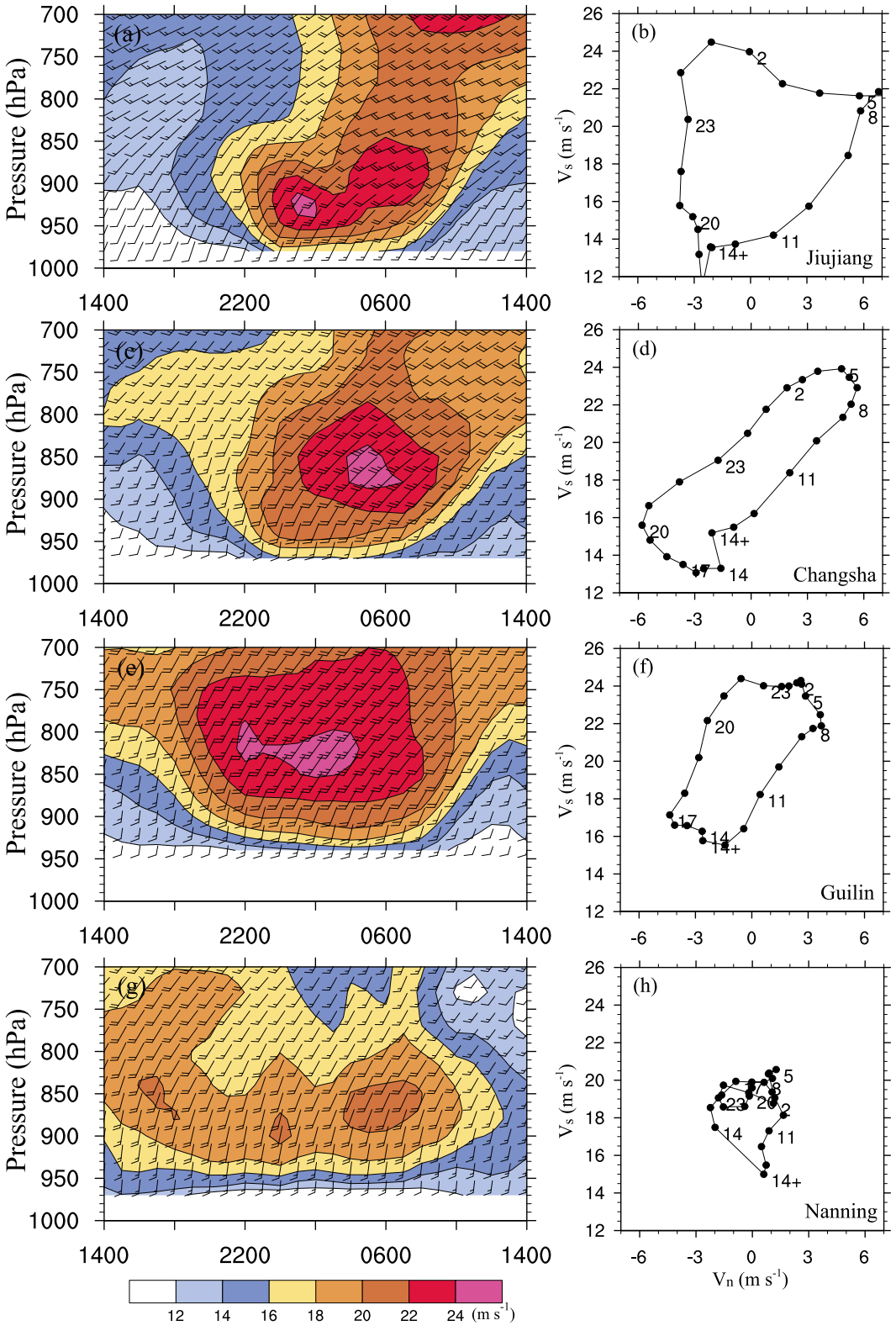

FIG. 6. As in Figs. 5a and 5c, but at (a),(b) JJ, (c),(d) CS, (e),(f) GL, and (g),(h) NN.

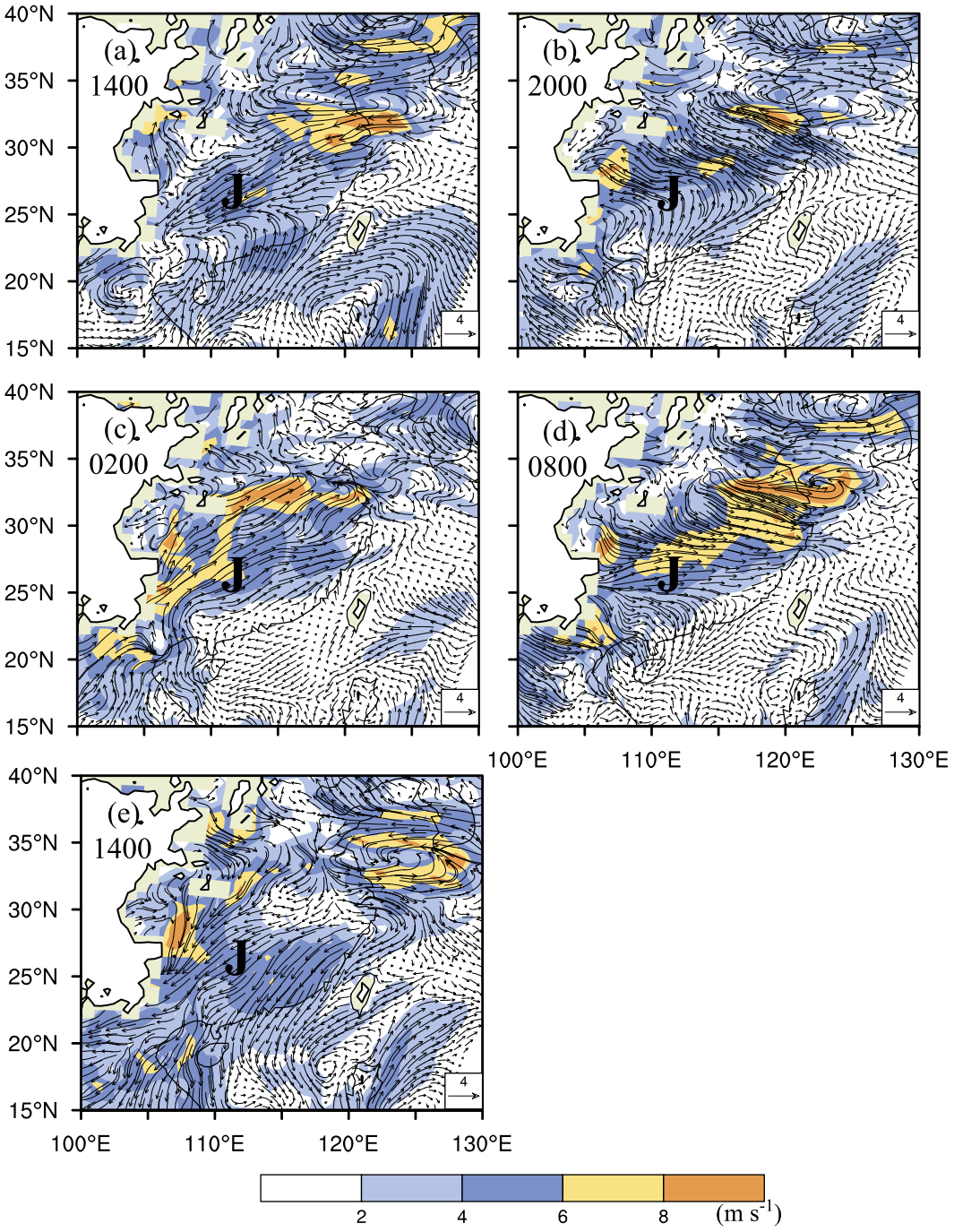

FIG. 7. Horizontal distribution of 850-hPa deviation wind vectors (relative to the daily averaged wind field; a scale of 4 m s^{-1} is given in the bottom-right corner) and speeds (shaded, m s^{-1}) from the WRF simulations, valid at (a) 1400 LST 29 Jun, (b) 2000 LST 29 Jun, (c) 0200 LST 30 Jun, (d) 0800 LST 30 Jun, and (e) 1400 LST 30 Jun 2003. Deviation wind speeds larger than 2 m s^{-1} are shaded at intervals of 2 m s^{-1}. The letter J marks the location of the LLJ core. Similar conventions apply for the following figures.

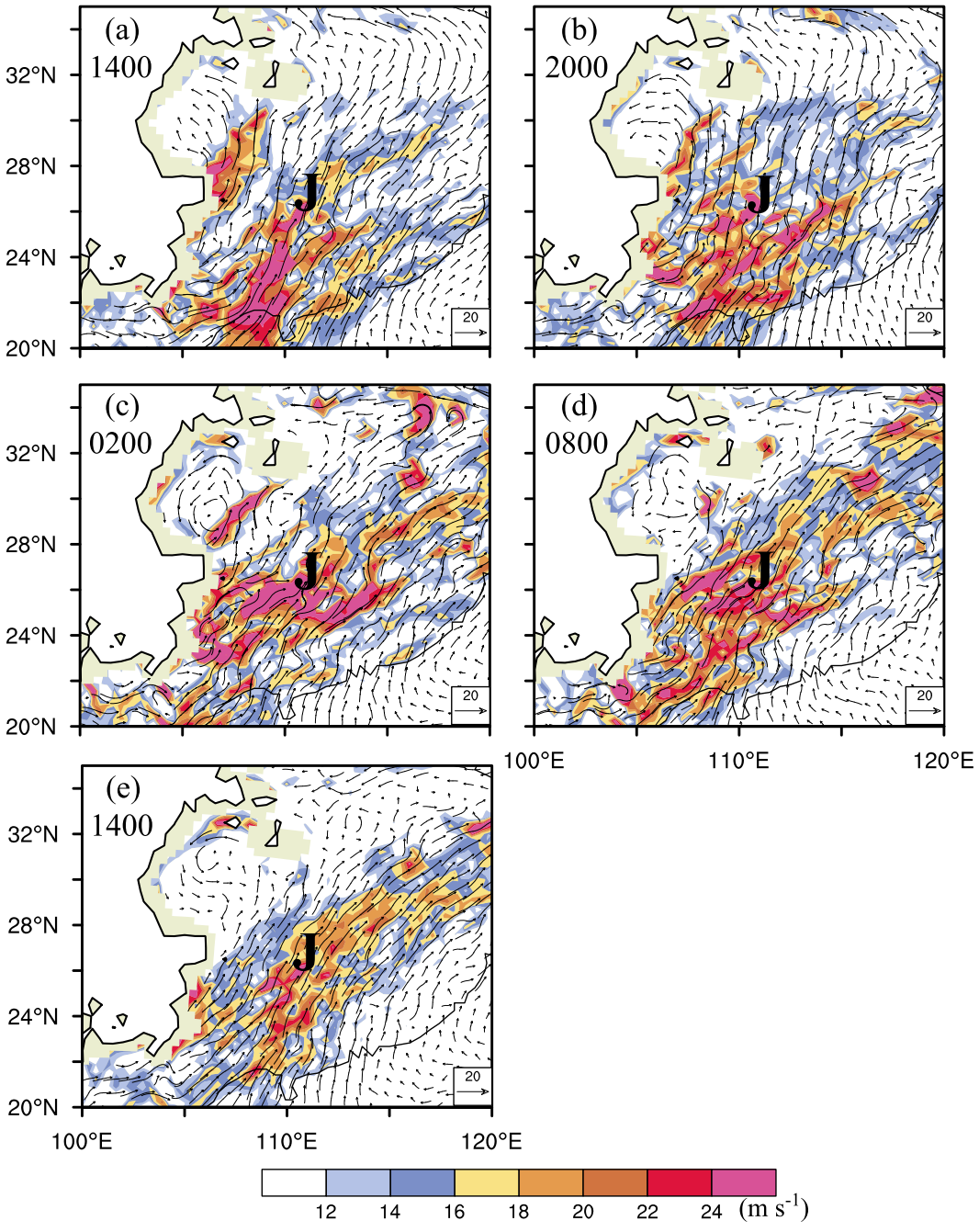

FIG. 8. Horizontal distribution of the 850-hPa geostrophic wind vectors (with a scale given in the bottom-right corner) and speeds (shaded, m s^{-1}) from the WRF simulation, valid at (a) 1400 LST 29 Jun, (b) 2000 LST 29 Jun, (c) 0200 LST 30 Jun, (d) 0800 LST 30 Jun, and (e) 1400 LST 30 Jun 2003. Wind speeds larger than 12 m s^{-1} are shaded at intervals of 2 m s^{-1}.

characteristics. In particular, the LLJ core during nighttime is nearly collocated with the local maximum $\mathbf{V}_{ag}$, reaching 16 m s^{-1} (cf. Figs. 9b–d and 2). Meanwhile, most ageostrophic winds along the LLJ axis are southwesterlies during nighttime (Figs. 9b,c) and northeasterlies during daytime (Figs. 9a,e), with westerlies to northwesterlies during the transition period (Fig. 9d). Such a diurnal variation of $\mathbf{V}_{ag}$ with clockwise rotation (or inertial oscillation) is also consistent with that of the horizontal wind deviations shown in Fig. 7. The magnitude of $\mathbf{V}_{ag}$ varies, too, peaking at 0200 and 0800 LST.

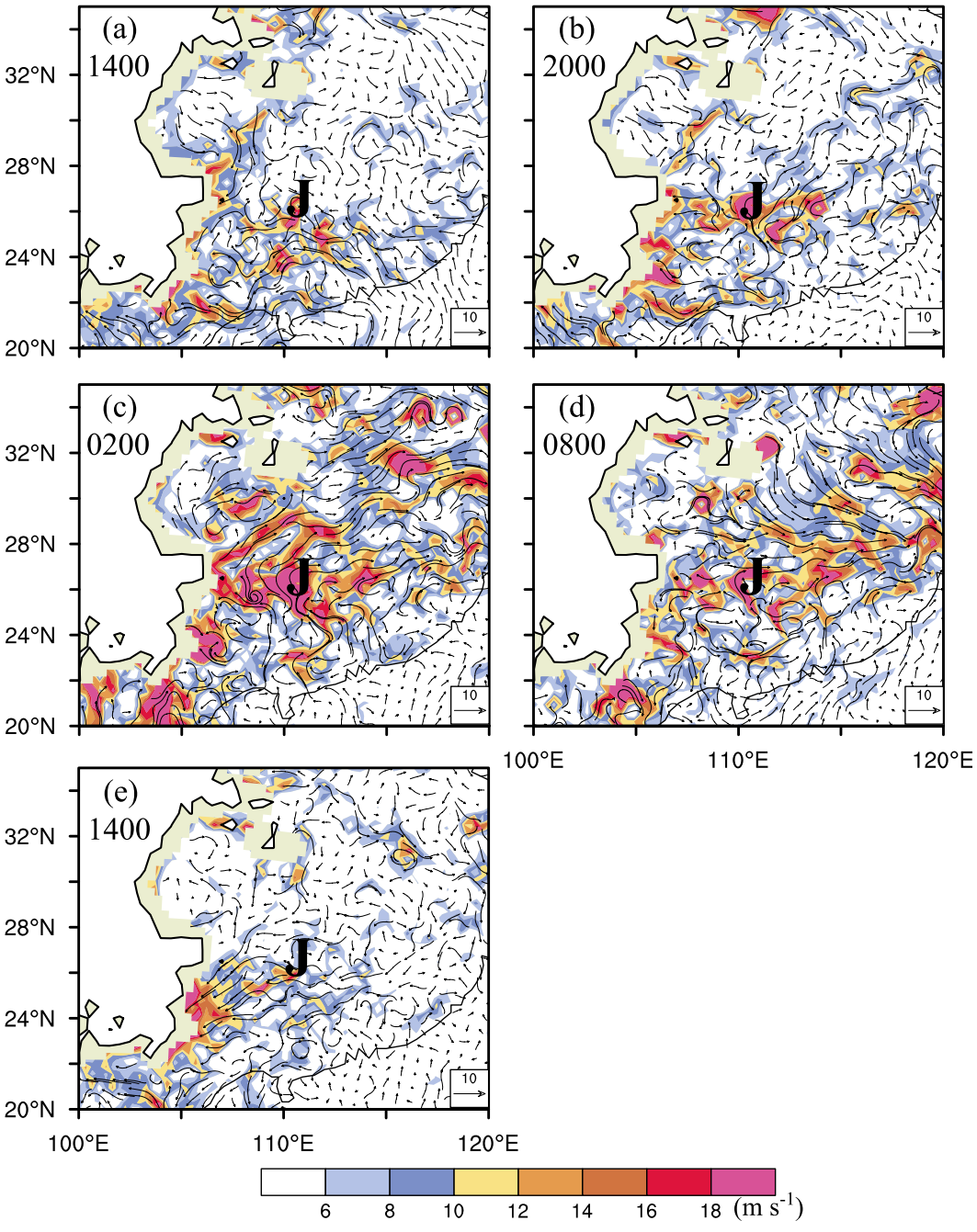

FIG. 9. As in Fig. 8, but for the ageostrophic wind field.

To better quantify the relative contributions of $\mathbf{V}_g$ and $\mathbf{V}_{ag}$ to the formation of the LLJ, we project the two wind components onto the LLJ coordinates. Clearly, it should be the wind speed along the s axis that contributes to the LLJ intensity. For this purpose, Fig. 10 shows the temporal variations of the geostrophic and ageostrophic wind speeds along the s and n axes at the LLJ core (i.e., at the Shaoyang station), while Fig. 11 presents their corresponding hodographs. Note that we have used the 6×6 grid (i.e., 72 km $\times$ 72 km) area averages to produce representative fields in Figs. 10–12. The s component V_{sg} of $\mathbf{V}_g$ experiences a sharp increase from 10.5 to 15.5 m s^{-1} during 2100–0200 LST, followed by a 12-h period of slow increases in the range of 15–17.5 m s^{-1} (Fig. 10). The sharp increase is consistent with that shown in Figs. 8 and 12a, and it results from the combined influences of

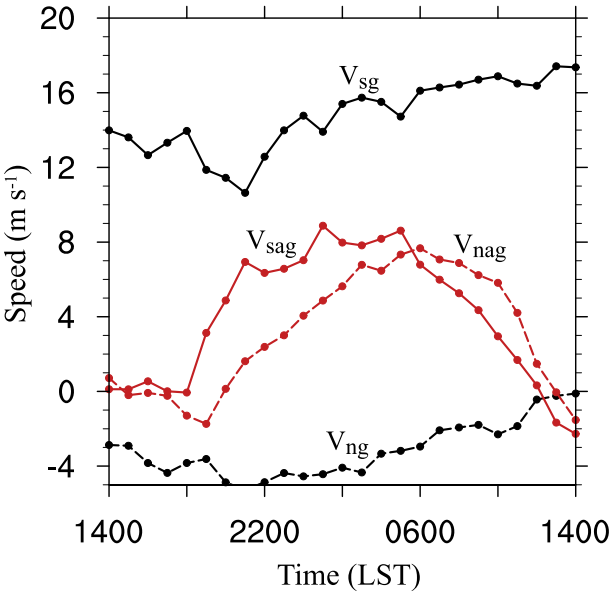

FIG. 10. Time series of the *s* axis (black solid line) and the *n* axis (black dashed lines) of $\mathbf{V}_g$, and the *s* axis (red solid line) and the *n* axis (red dashed lines) of $\mathbf{V}_{ag}$ at 850 hPa at SY from the 24-h (1400 LST 29 June–1400 LST 30 June) WRF simulation, which are obtained by averaging each variable over an area of 72 km × 72 km at each hour.

large-scale flows and the reversed temperature gradients normal to the Yun-Gui Plateau. The subsequent gradual increase of V_{sg} may be attributed to the northwestward extension of the WPSH, which enhances the pressure gradient force, as indicated in Fig. 12a.

In spite of a few large oscillations, geostrophic winds vary more along the *s* axis (e.g., in the range of 10–18 m s^{-1}) with little changes (−5–0 m s^{-1}) in the normal component or wind direction (Fig. 11a). By comparison, the ageostrophic counterpart exhibits pronounced diurnal variations in both amplitude and direction, with clear clockwise rotation along an inertial circle at a radius of about 5.5 m s^{-1} (Fig. 11b). In particular, the *s* component of $\mathbf{V}_{ag}$ increases with time in the late afternoon and reaches its maximum of 9 m s^{-1} at 0100 LST. If the $\mathbf{V}_g$ (~15 m s^{-1}) and $\mathbf{V}_{ag}$ (~8 m s^{-1}) contributions along the *s* axis are compared to those at 0200 LST, when the LLJ is peaked, the former accounts for about 65% of the peak strength of the LLJ at its core region. Of course, not all of the $\mathbf{V}_g$ contributions should be attributed to the large-scale pressure system because of the effects of the diurnal heating cycle associated with the Yun-Gui Plateau. Nevertheless, the above results indicate that the intense southwesterly flow could be considered to be an LLJ stream in the absence of the diurnal heating cycles, since the large-scale pressure system can produce a sizeable portion of the LLJ

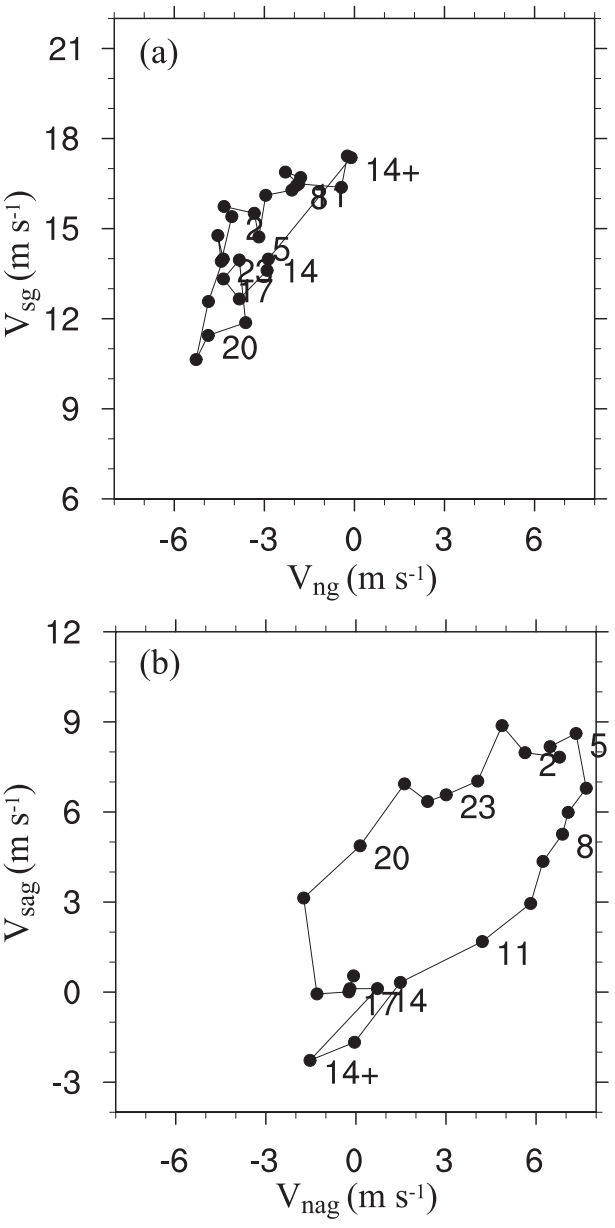

FIG. 11. Hodographs (m s^{-1}) of the (a) geostrophic and (b) ageostrophic wind fields taken at hourly intervals at 850 hPa at SY from the 24-h (1400 LST 29 June–1400 LST 30 June) WRF simulation. Hodographs are obtained by averaging each variable over an area of 72 km × 72 km at each hour.

intensity. The amplitudes of both the geostrophic deviations and the inertial cycle decrease rapidly upward (not shown).

Du et al. (2015a) simulated the PBL jets (~925 hPa) off the southeastern coast of China, and found that the geostrophic winds account for about 87% of the total wind speeds. As will be shown in section 4b, the relative larger contribution of $\mathbf{V}_{ag}$ in our case (35%) could be

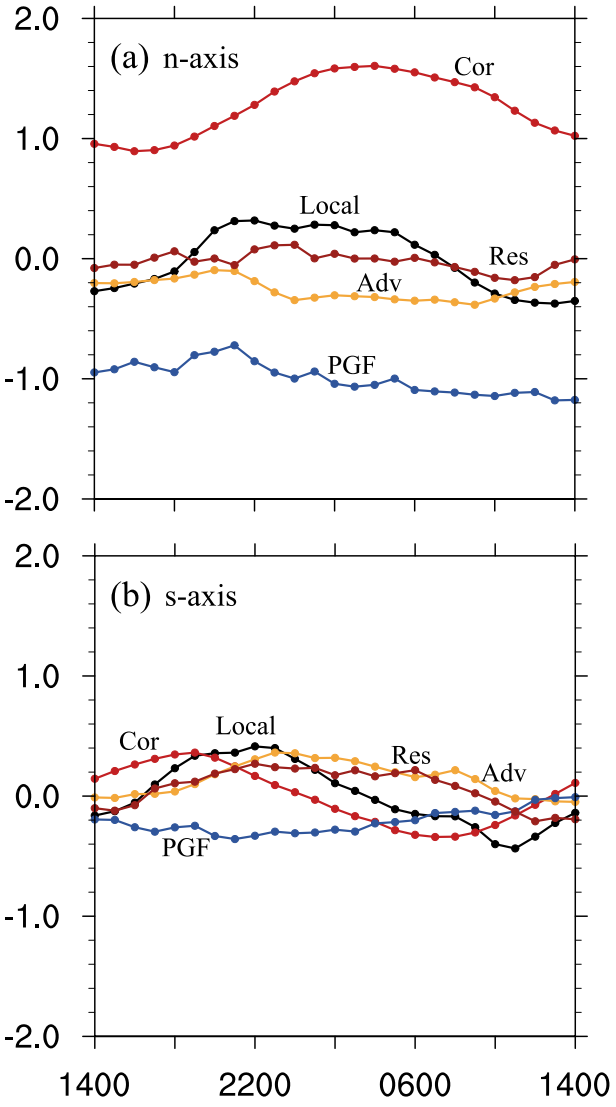

FIG. 12. Time series of the local rates of changes of the horizontal wind speed (black; Local), the horizontal advection (yellow; Adv), the Coriolis force (red; Cor), the pressure gradient force (blue; PGF), and the residue term (brown; Res) along (a) the n and (b) s axes, from the 24-h (1400 LST 29 June–1400 LST 30 June) WRF simulation. Time series are obtained by averaging each term over an area of 72 km × 72 km at each hour. The unit is $10^{-3}\,\mathrm{m\,s^{-2}}$.

attributed mostly to the surface heating cycle (i.e., Blackadar's mechanism), which is of little importance over oceans (Du et al. 2015b).

c. *Unbalanced characteristics of the LLJ*

After seeing the relative contributions of $\mathbf{V}_g$ and $\mathbf{V}_{ag}$ along the s axis, we may use the following horizontal momentum equations in the LLJ coordinates to examine the unbalanced characteristics of the LLJ at its core region:

$$\frac{\partial V_n}{\partial t} = (-\mathbf{V}\cdot\nabla\mathbf{V})_n + fV_s - \frac{\partial\Phi}{\partial n} + \text{Residue} \quad \text{and} \quad (1)$$

$$\frac{\partial V_s}{\partial t} = (-\mathbf{V}\cdot\nabla\mathbf{V})_s - fV_n - \frac{\partial\Phi}{\partial s} + \text{Residue}, \quad (2)$$

where $\partial V_n/\partial t$ and $\partial V_s/\partial t$ denote the local rate of change of the horizontal wind along the respective n and s axes, and the right-hand-side terms from left to right are the horizontal advection, the Coriolis force, the pressure gradient force, and the residue, respectively. Because the jet core is far away from the rain belt, the vertical advection is small and the frictional force is dominant in the residue term.

Figure 12 shows the temporal evolution of each item in Eqs. (1) and (2) at 850 hPa at SY. We see that for the n-axis component the advection and residue terms are much smaller than the other two forcing terms so the local rates of changes in $\mathbf{V}_n$ yield small differences between the Coriolis and pressure gradient forces (Fig. 12a). This gives rise to the radius of inertial oscillation, that is, $f\,(\mathbf{V} - \mathbf{V}_g)$, implying that the latter two large terms contribute to the formation of the LLJ. Because the pressure gradient force increases slowly with time in association with the northwestward progression of the WPSH, the n-axis ageostrophic acceleration is nearly in phase with the Coriolis force, and it begins to increase near 1800 LST, as is also shown in Fig. 5a, reaching its peak amplitude near 0200 LST. This peak amplitude occurs ahead of that in $\mathbf{V}_{nag}$ (0600 LST), as seen in Fig. 11, showing the important roles of unbalanced forcing in generating large $\mathbf{V}_{nag}$ during the early morning hours. In contrast, the local rates of change in V_s are similar in magnitude to those of the Coriolis and pressure gradient forces as well as the advection and residue terms along the s axis, but with some phase differences. This indicates that the along-LLJ axis component is dominated by the balanced synoptic-scale flows and enhanced by the diurnal heating cycle associated with the Yun-Gui Plateau.

4. Sensitivity simulations

a. *Experimental design*

Previous studies have shown the importance of solar radiation, surface heat flux, topography, latent heat release, and the land–sea contrast in the formation of LLJs (e.g., Zhang et al. 2006; Saulo et al. 2007). However, their relative impacts are case dependent, with some parameters being more significant than others. For example, Du et al. (2015a) showed that the land–sea thermal contrast dominates the formation of the boundary layer jet off the southeastern coast of China.

TABLE 1. WRF experimental design.

Index	Expt	Expt description
0	CTL	The full-physics run with realistic topography
1	NORAD	Long- and shortwave radiation turned off
2	NOTP	Any elevation higher than 1200 m over the Tibetan Plateau is shaved
3	NOYG	Any elevation higher than 50 m over the Yun-Gui Plateau is shaved
4	NOSM	Any elevation higher than 50 m over the southeastern mountains is shaved
5	NOLH	Latent heat release associated with cloud microphysics and the cumulus parameterization scheme turned off

Thus, in this section, a series of five sensitivity experiments is carried out to examine the relative contributions of the aforementioned factors to the formation of the LLJ, using the results presented in section 3 as the control run (CTL). Specifically, experiments NORAD, NOTP, NOYG, NOSM, and NOLH are designed to test the effects of no radiation; shaving off some top portion of the topography associated with the Tibetan Plateau, Yun-Gui Plateau, and southeastern mountains; and no condensational heating, respectively, on the formation of the present LLJ (see Table 1 for more details).

Some special considerations for shaving off terrain heights are mentioned below. In experiment NOTP, because the average elevation of the Yun-Gui Plateau is about 1200 m, any elevation higher than 1200 m is shaved off while keeping the lower-elevation terrain untouched in order to minimize the terrain-gradient-induced thermal gradients. Similarly, the Yun-Gui Plateau and southeastern mountains are shaved to 50 m in experiments NOYG and NOSM, respectively, because of the average plain elevation of around 50 m over east China.

b. *Effect of turning off surface radiation*

Because the model is initialized in the morning with lower ground temperatures, the PBL in this experiment receives little heating in the presence of surface heat fluxes after turning off the solar and infrared radiation. Without the surface radiative forcing (NORAD), the southwesterly winds at 850 hPa, where the LLJ in CTL is peaked, weaken significantly in intensity and shrink in their area of coverage. That is, the maximum wind speed in the core region is 4–6 m s^{-1} weaker than that in CTL (Fig. 13a), and a jetlike vertical structure does not appear at all five of the stations (Fig. 13b). This can be seen from the time–height cross section of horizontal winds and the hodograph at Shaoyang station in Figs. 13c and 13d, showing that the vertical structures of horizontal winds change only slightly from those at the model initial time. Thus, there is little evidence of LLJ development compared to that in CTL (cf. Figs. 13c and 5a). Meanwhile, there is little evidence of inertial oscillation in the hodograph of horizontal winds at the core region (cf. Figs. 13d and 5c).

Turning off the surface radiation results in the absence of both diurnal eddy mixing in the PBL (i.e., Blackadar's mechanism) and thermal contrasts between mountains and valleys (i.e., Holton's mechanism). This result is similar to that obtained in an experiment in which surface heat fluxes are turned off (not shown). As a result the southwesterly flow decreases in amplitude by as much as 6–12 m s^{-1} over the sloping terrains closely along the eastern and northeastern edges of the Yun-Gui Plateau (Fig. 14a). These results are consistent with the findings of Zhang et al. (2006) and the theories of both Blackadar (1957) and Holton (1967) in that the surface heating is crucial for the formation of the nocturnal LLJ.

c. *Effect of shaving off terrain heights*

As compared with the effects of the surface heating, shaving off the upper portion of the Tibetan Plateau, the Yun-Gui Plateau, and the southeastern mountains in experiments NOTP, NOYG, and NOSM, respectively, produces much less impact on the formation of the LLJ. Namely, the major LLJ characteristics are still present but with weaker LLJ intensities. Among the three sensitivity experiments, shaving off the Yun-Gui Plateau appears to have a more pronounced impact of the intensity of the LLJ. This result may be expected in some sense, given the close location of the LLJ core with respect to the Yun-Gui Plateau. Thus, we only plot results from experiment NOYG.

Unlike the results in NORAD, differences in the horizontal winds between CTL and NOYG mainly appear to the west of 115°E, and the wind speed at the LLJ core is about 6–10 m s^{-1} weaker than that in CTL (Fig. 14b). Likewise, vertical wind profiles taken along the LLJ axis are all similar to those in CTL, albeit with smaller magnitudes (cf. Figs. 15b and 3b). The LLJ at SY is also notably weaker in amplitude and shorter in duration, but still shows well the typical LLJ characteristics (Fig. 15c). Of importance is that the weakening of the LLJ core occurs mainly along the s axis and its s-component V_s, with small changes in V_n (cf. Figs. 15d and 5c).

Shaving off the terrain heights of the Yun-Gui Plateau results in the reduction of both the diurnal thermal

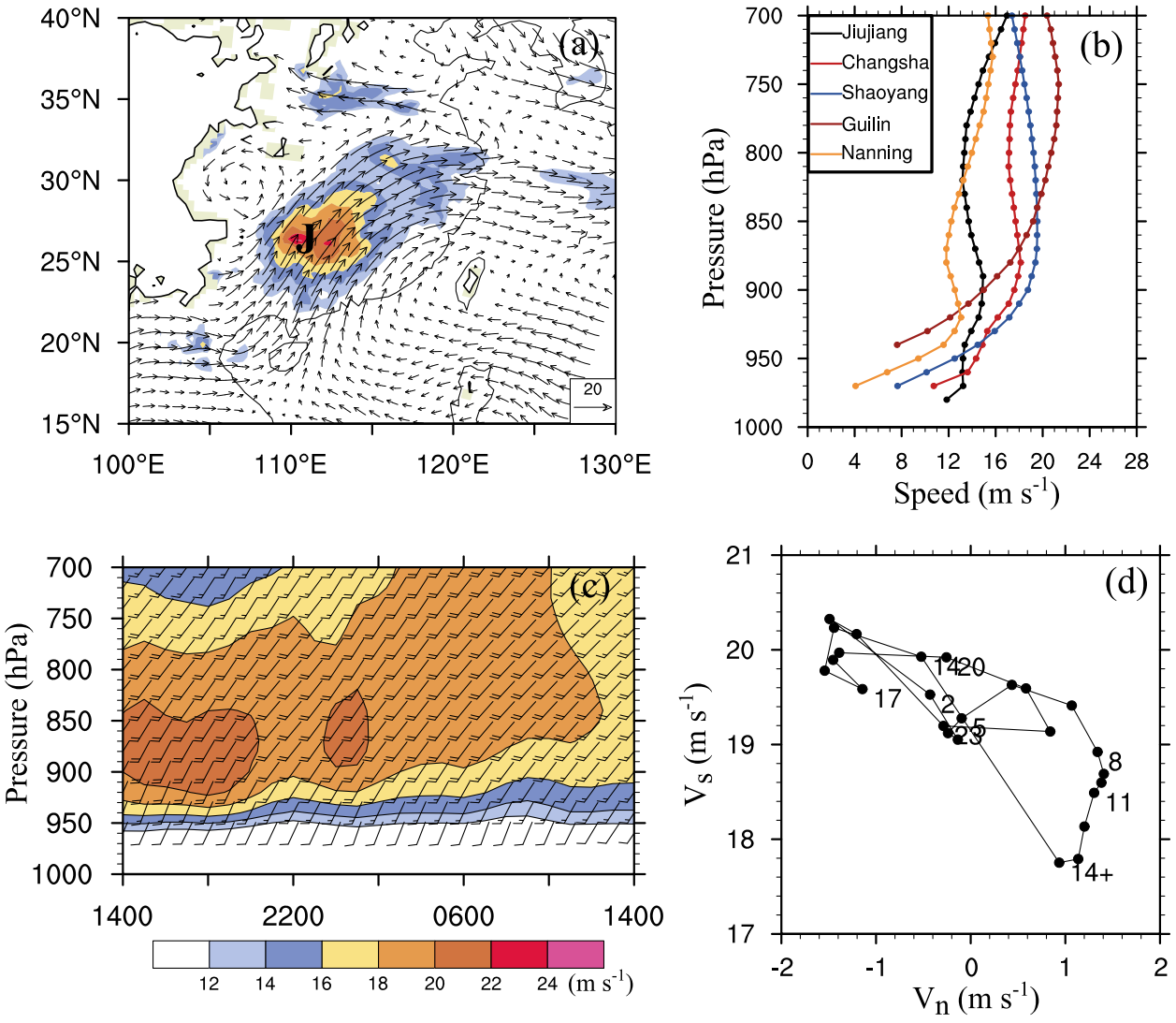

FIG. 13. (a) As in Fig. 2b, (b) as in Fig. 3b, (c) as in Fig. 5a, and (d) as in Fig. 5c, but for experiment NORAD (i.e., in the absence of the surface radiative heating). Note that a different scale is used for the hodograph in (d).

forcing effect and the dynamic blocking effect. That is, removing the Yun-Gui Plateau weakens the diurnal variation of east–west temperature gradients (not shown), and also the intensity of the cyclonic vortex over the Sichuan basin (Fig. 14b), leading to decreases in V_{sg}. Therefore, the decreased *s*-component of $\mathbf{V}_g$ should contain both the thermal forcing and dynamic effects. Based on this sensitivity simulation, we may state that the surface diurnal heating cycle and the blocking effect associated with the Yun-Gui Plateau play a secondary role in the formation of the present LLJ, and the Tibet Plateau and the southeastern mountains produce little impact. Our findings are similar to those of Du et al. (2015a), who also find that the terrain of Taiwan and Fujian exerts a secondary influence on the strength of the coastal boundary layer jet off the southeastern coast of China.

d. Effect of turning off latent heat release

In the absence of latent heat release in experiment NOLH, the cyclonic wind shear and convergence along the mei-yu front (near 33°N) become insignificant (cf. Figs. 16a and 2b, Fig. 14c). The coverage of the LLJ (i.e., larger than $12\,\mathrm{m\,s^{-1}}$) decreases, similarly for the peak intensity in the core region (cf. Figs. 16 and 2b, 3b and 5a). All these findings imply that condensational heating along the mei-yu front acts to increase the southwesterly component of the LLJ. At some locations close to the mei-yu front, the southwesterly wind speeds weaken by as much as 8–$10\,\mathrm{m\,s^{-1}}$. However, differences in wind

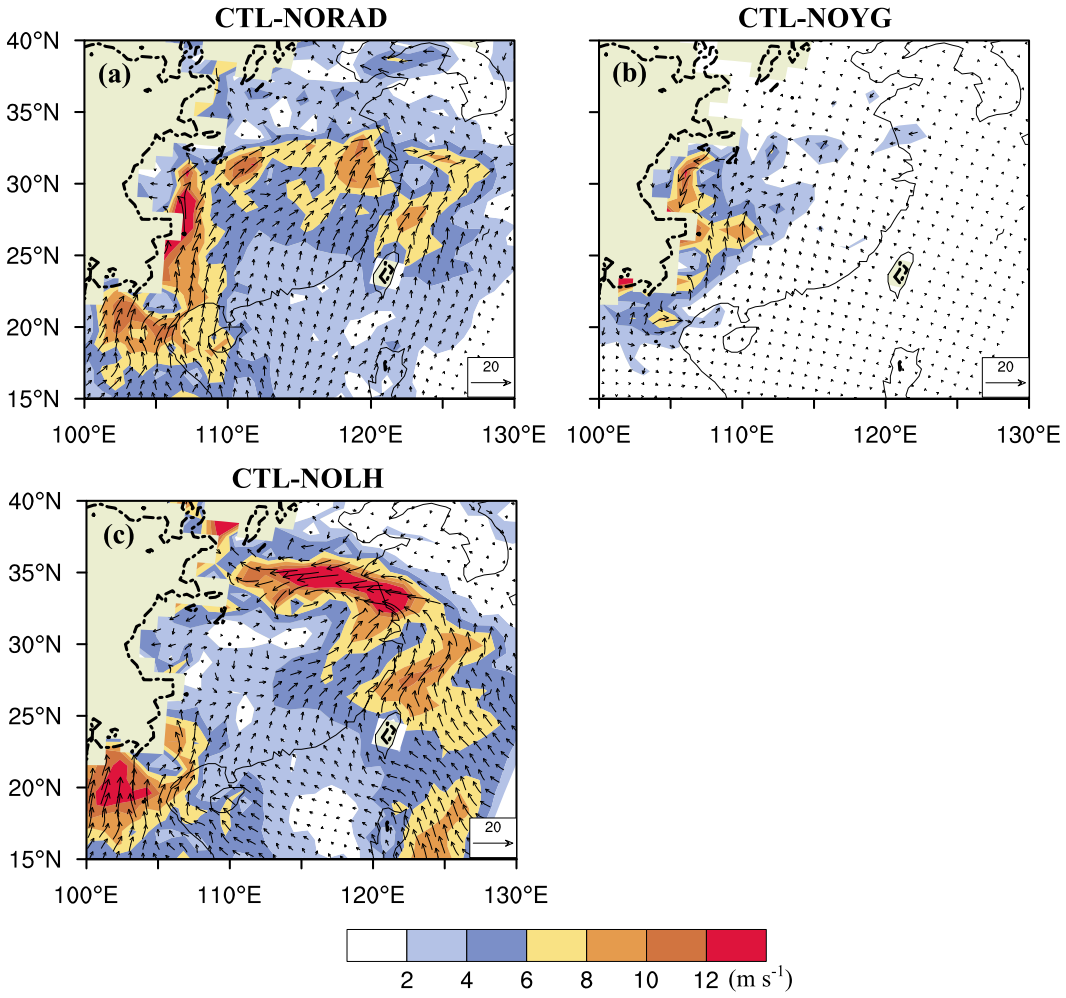

FIG. 14. Differences in 850-hPa wind vectors and speeds between the (a) CTL and NORAD simulations, (b) CTL and NOYG simulations, and (c) CTL and NOLH simulations, valid at 0200 LST 30 Jun 2003.

speed along the LLJ axis between CTL and NOLH are relatively small at the locations that are far away from the mei-yu frontal rainbelt (e.g., only 2–4 m s^{-1} near the jet core; see Fig. 14c). This result is consistent with the findings of Qian et al. (2004) that although the LLJ is mostly determined by the large-scale pressure system, mesoscale circulations resulting from latent heat release could enhance the magnitude of the LLJ, more evidently in the regions close to heavy precipitation. This enhancement can be achieved through secondary circulations associated with the latent heating–induced convergence in the lower troposphere, as also investigated by Chen et al. (1994, 2006).

Like the horizontal structures, the vertical jetlike profile of the horizontal wind speed near the mei-yu front (e.g., JJ) becomes flatter in the absence of latent heat release, whereas the other stations far away from this region (e.g., SY, GL, and NN) exhibit vertical profiles that are similar to those in CTL (cf. Figs. 16b and 3b). Diurnal variations of the LLJ core at SY become less pronounced than those in CTL in both amplitude and direction (cf. Figs. 16c,d and 5a,c). The diurnal variation amplitudes of the along V_s and normal V_n components of the horizontal wind in the core region are 6 and 5 m s^{-1}, respectively, as compared to 11 m s^{-1} in CTL (cf. Figs. 16d and 5c). This means that latent heat release along the mei-yu front, though 500–600 km away, still play some role in determining the intensity of the LLJ.

5. Summary and concluding remarks

In this study, a warm season LLJ event occurring on the eastern foothills of the Yun-Gui Plateau in south China during a 24-h period from 1400 LST 29 June to 1400 LST 30 June 2003 is examined with both the NCEP

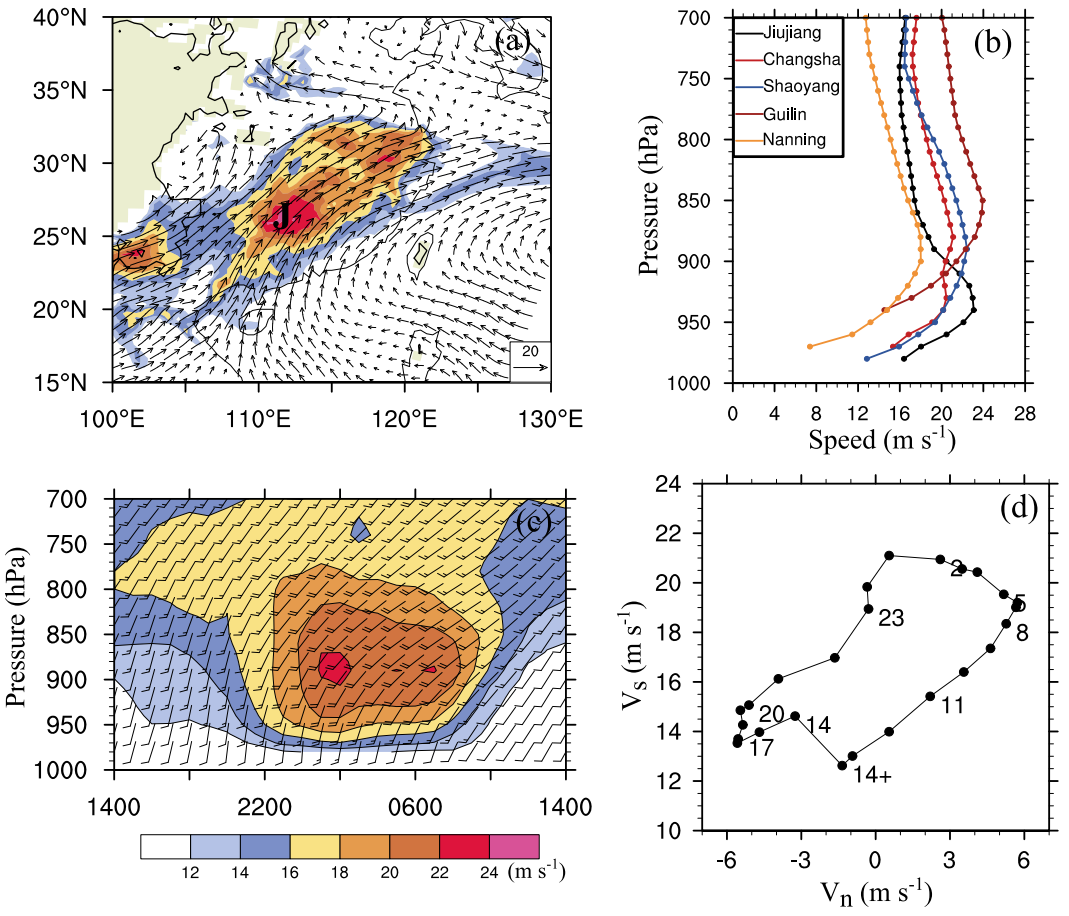

FIG. 15. As in Fig. 13, but for experiment NOYG (i.e., shaving off the Yun-Gui Plateau). Note that when shaving off the Yun-Gui Plateau, the southwesterly flows can sweep over the area higher than 1500 m over region 2 in Fig. 1.

FNL analysis data and high-resolution WRF Model simulations. The major portion of the LLJ ($\geq$16 m s^{-1}) closely followed the eastern foothills of the Yun-Gui Plateau. The southwesterly LLJ with ample water vapor was converged along a mei-yu front near 33°N, where heavy rainfall occurred. A western Pacific subtropical high and a mesoscale low pressure system (i.e., southwest vortex) on the respective southeast and northwest sides of the LLJ provided a favorable background pressure field for the LLJ development.

The low-level wind field is characterized by significant diurnal variations with vertical jet profiles occurring after midnight, and wind speeds reaching their peak intensity of greater than 24 m s^{-1} at 850 hPa in the core region. Meanwhile, horizontal wind directions below 800 hPa veer from southerly before sunset to southwesterly during the nighttime. An LLJ coordinates system is proposed, in which both the along- and the normal-to-LLJ components (V_s and V_n, respectively) of the horizontal wind have a diurnal variation (with clockwise rotation) of about 11 m s^{-1} during the 24-h period, which is consistent with Blackadar's inertial oscillation theory.

Results show that the along-LLJ geostrophic winds $\mathbf{V}_g$ dominate the distribution (or location) of the LLJ with small directional shifts throughout the 24-h period. The diurnal variations of the along-LLJ $\mathbf{V}_g$ intensity are closely related to the increased horizontal pressure gradient due to the northwestward extension of WPSH, and enhanced by the diurnal heating cycle associated with the sloping topography. In contrast, the ageostrophic winds $\mathbf{V}_{ag}$ contribute to the clockwise rotation of horizontal winds, thus leading to the formation and weakening of the LLJ during the night- and daytime, respectively. It is found that $\mathbf{V}_g$ and $\mathbf{V}_{ag}$ along the LLJ axis account for about 65% and 35%, respectively, of the peak intensity of the LLJ at its core region at 0200 LST.

A series of numerical sensitivity experiments is conducted, which confirms that the radiation (similar to surface heating) is the key factor in determining the formation of the nocturnal LLJ. Without the solar and infrared radiation, the low-level southwesterly winds

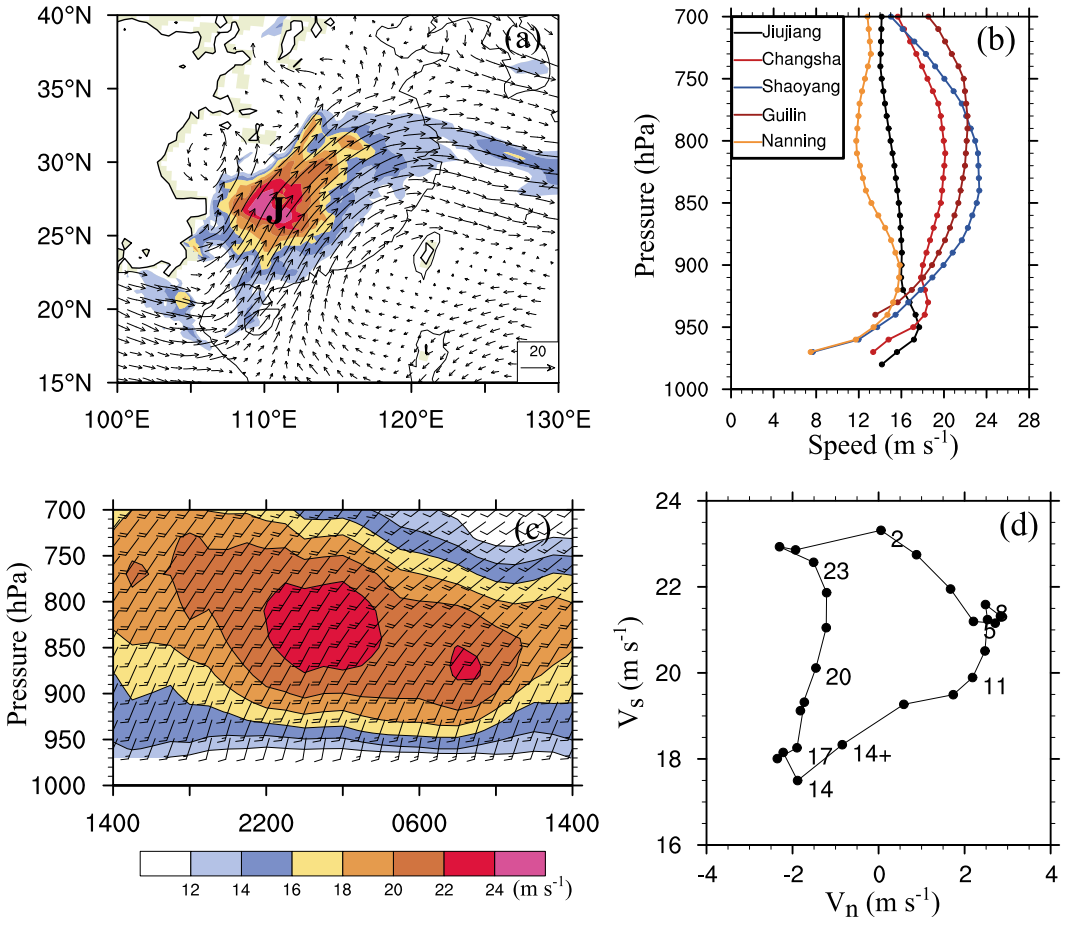

FIG. 16. As in Fig. 13, but for experiment NOLH (i.e., in the absence of latent heat release).

weaken significantly with little evidence of the jetlike structure in the vertical. When the Yun-Gui Plateau is shaved off, the southwest vortex over the Sichuan basin is weakened as a result of removing the plateau's blocking effects. The resulting decreases in both the pressure gradient force and the temperature gradients between the Yun-Gui Plateau and the southeastern mountains (plains) weaken the intensity of the LLJ. The results show that shaving off the Yun-Gui Plateau and the downstream condensational heating along the mei-yu front play secondary roles in the formation of the LLJ. Shaving off the terrain height of the Tibetan Plateau and southeastern mountains shows the least influence.

In conclusion, the eastern foothills of the Yun-Gui Plateau appear to be a favorable region for the formation of LLJs, given the presence of typical southwesterly monsoonal flows during the warm season. It should be mentioned that the evolution of low-level winds, including LLJs, and their relation to warm season rainfall over south China are far more complicated than those discussed herein because of the influences of complex terrain associated with the Tibetan Plateau, the Yun-Gui Plateau, and the southeastern mountains. Clearly, more case studies are needed to generalize the above results, especially those related to the impact of complex terrain and the roles of LLJs in the generation of heavy rainfall.

Acknowledgments. We thank three anonymous reviewers for their constructive comments. This work is jointly supported by the National Basic Research Program of China (973 Program, Grant 2015CB954102), the National Natural Science Foundation of China (Grants 41475043 and 41205079), and the China Meteorological Administration for the R&D Special Fund for Public Welfare Industry (Meteorology) (Grant GYHY201306016).

REFERENCES

Archer, C. L., and M. Z. Jacobson, 2005: Evaluation of global wind power. *J. Geophys. Res.*, **110**, D12110, doi:10.1029/2004JD005462.

Ardanuy, P., 1979: On the observed diurnal oscillation of the Somali jet. *Mon. Wea. Rev.*, **107**, 1694–1700, doi:10.1175/1520-0493(1979)107<1694:OTODOO>2.0.CO;2.

Arritt, R. W., T. D. Rink, M. Segal, D. P. Todey, C. A. Clark, M. J. Mitchell, and K. M. Labas, 1997: The Great Plains low-level jet during the warm season of 1993. *Mon. Wea. Rev.*, **125**, 2176–2192, doi:10.1175/1520-0493(1997)125<2176:TGPLLJ>2.0.CO;2.

Blackadar, A. K., 1957: Boundary layer wind maxima and their significance for the growth of nocturnal inversions. *Bull. Amer. Meteor. Soc.*, **38**, 283–290.

Bonner, W. D., and J. Paegle, 1970: Diurnal variations in boundary layer winds over the south-central United States in summer. *Mon. Wea. Rev.*, **98**, 735–744, doi:10.1175/1520-0493(1970)098<0735:DVIBLW>2.3.CO;2.

Chen, F., and J. Dudhia, 2001: Coupling an advanced land surface–hydrology model with the Penn State–NCAR MM5 modeling system. Part I: Model description and implementation. *Mon. Wea. Rev.*, **129**, 569–585, doi:10.1175/1520-0493(2001)129<0569:CAALSH>2.0.CO;2.

Chen, G. T.-J., C.-C. Wang, and L.-F. Lin, 2006: A diagnostic study of a retreating mei-yu front and the accompanying low-level jet formation and intensification. *Mon. Wea. Rev.*, **134**, 874–896, doi:10.1175/MWR3099.1.

Chen, Y.-L., X. A. Chen, and Y.-X. Zhang, 1994: A diagnostic study of the low-level jet during TAMEX 5. *Mon. Wea. Rev.*, **122**, 2257–2284, doi:10.1175/1520-0493(1994)122<2257:ADSOTL>2.0.CO;2.

Ding, Y., 1994: *Monsoons over China.* Kluwer Academic, 419 pp.

——, J.-J. Liu, Y. Sun, Y.-J. Liu, H.-H. He, and Y.-F. Song, 2007: A study of the synoptic-climatology of the Meiyu system in East Asia (in Chinese). *Chin. J. Atmos. Sci.*, **31**, 1082–1101.

Douglas, M. W., 1995: The summertime low-level jet over the Gulf of California. *Mon. Wea. Rev.*, **123**, 2334–2347, doi:10.1175/1520-0493(1995)123<2334:TSLLJO>2.0.CO;2.

Du, Y., and R. Rotunno, 2014: A simple analytical model of the nocturnal low-level jet over the Great Plains of the United States. *J. Atmos. Sci.*, **71**, 3674–3683, doi:10.1175/JAS-D-14-0060.1.

——, Q. H. Zhang, Y. Yue, and Y. Yang, 2012: Characteristics of low-level jets in Shanghai during the 2008-2009 warm seasons as inferred from wind profiler radar data. *J. Meteor. Soc. Japan*, **90**, 891–903, doi:10.2151/jmsj.2012-603.

——, ——, Y.-L. Chen, Y. Zhao, and X. Wang, 2014: Numerical simulations of spatial distributions and diurnal variations of low-level jets in China during early summer. *J. Climate*, **27**, 5747–5767, doi:10.1175/JCLI-D-13-00571.1.

——, Y.-L. Chen, and Q. Zhang, 2015a: Numerical simulations of the boundary layer jet off the southeastern coast of China. *Mon. Wea. Rev.*, **143**, 1212–1231, doi:10.1175/MWR-D-14-00348.1.

——, R. Rotunno, and Q. Zhang, 2015b: Analysis of WRF-simulated diurnal boundary layer winds in eastern China using a simple 1D model. *J. Atmos. Sci.*, **72**, 714–727, doi:10.1175/JAS-D-14-0186.1.

Dudhia, J., 1989: Numerical study of convection observed during the Winter Monsoon Experiment using a mesoscale two-dimensional model. *J. Atmos. Sci.*, **46**, 3077–3107, doi:10.1175/1520-0469(1989)046<3077:NSOCOD>2.0.CO;2.

Farquharson, J. S., 1939: The diurnal variation of wind over tropical Africa. *Quart. J. Roy. Meteor. Soc.*, **65**, 165–184, doi:10.1002/qj.49706528004.

Ferrier, B. S., Y. Lin, T. Black, E. Rogers, and G. DiMego, 2002: Implementation of a new grid-scale cloud and precipitation scheme in the NCEP Eta model. Preprints, *15th Conf. on Numerical Weather Prediction*, San Antonio, TX, Amer. Meteor. Soc., 280–283.

Goualt, J., 1938: Vents en altitude a fort Lamy (Tchad). *Ann. Phys. Globe France d'Outre-Mer*, **5**, 70–91.

Higgins, R., Y. Yao, E. Yarosh, J. E. Janowiak, and K. Mo, 1997: Influence of the Great Plains low-level jet on summertime precipitation and moisture transport over the central United States. *J. Climate*, **10**, 481–507, doi:10.1175/1520-0442(1997)010<0481:IOTGPL>2.0.CO;2.

Holton, J. R., 1967: The diurnal boundary layer wind oscillation above sloping terrain. *Tellus*, **19**, 199–205, doi:10.1111/j.2153-3490.1967.tb01473.x.

Kain, J. S., 2004: The Kain–Fritsch convective parameterization: An update. *J. Appl. Meteor.*, **43**, 170–181, doi:10.1175/1520-0450(2004)043<0170:TKCPAU>2.0.CO;2.

Liechti, F., and E. Schaller, 1999: The use of low-level jets by migrating birds. *Naturwissenschaften*, **86**, 549–551, doi:10.1007/s001140050673.

Liu, H., D.-L. Zhang, and B. Wang, 2008: Daily to submonthly weather and climate characteristics of the summer 1998 extreme rainfall over the Yangtze River basin. *J. Geophys. Res.*, **113**, D22101, doi:10.1029/2008JD010072.

——, L.-J. Li, and B. Wang, 2012: Low-level jets over southeast China: The warm season climatology of the summer of 2003. *Atmos. Oceanic Sci. Lett.*, **5**, 394–400, doi:10.1080/16742834.2012.11447017.

Liu, X., and Y. Jiao, 2000: Sensitivity of the East Asian monsoon climate to the Tibetan Plateau uplift (in Chinese). *Chin. J. Atmos. Sci.*, **24**, 593–607.

Maddox, R. A., 1980: Mesoscale convective complexes. *Bull. Amer. Meteor. Soc.*, **61**, 1374–1387, doi:10.1175/1520-0477(1980)061<1374:MCC>2.0.CO;2.

Muñoz, R. C., and R. D. Garreaud, 2005: Dynamics of the low-level jet off the west coast of subtropical South America. *Mon. Wea. Rev.*, **133**, 3661–3677, doi:10.1175/MWR3074.1.

Nakanishi, M., and H. Niino, 2006: An improved Mellor–Yamada level-3 model: Its numerical stability and application to a regional prediction of advection fog. *Bound.-Layer Meteor.*, **119**, 397–407, doi:10.1007/s10546-005-9030-8.

Qian, J.-H., W.-K. Tao, and K. Lau, 2004: Mechanisms for torrential rain associated with the mei-yu development during SCSMEX 1998. *Mon. Wea. Rev.*, **132**, 3–27, doi:10.1175/1520-0493(2004)132<0003:MFTRAW>2.0.CO;2.

Rife, D. L., J. O. Pinto, A. J. Monaghan, C. A. Davis, and J. R. Hannan, 2010: Global distribution and characteristics of diurnally varying low-level jets. *J. Climate*, **23**, 5041–5064, doi:10.1175/2010JCLI3514.1.

Rogers, E., T. Black, B. Ferrier, Y. Lin, D. Parrish, and G. DiMego, 2001: Changes to the NCEP Meso Eta Analysis and Forecast System: Increase in resolution, new cloud microphysics, modified precipitation assimilation, modified 3DVAR analysis. NWS Tech. Procedures Bulletin. [Available online at http://www.emc.ncep.noaa.gov/mmb/mmbpll/eta12tpb/.]

Saulo, C., J. Ruiz, and Y. G. Skabar, 2007: Synergism between the low-level jet and organized convection at its exit region. *Mon. Wea. Rev.*, **135**, 1310–1326, doi:10.1175/MWR3317.1.

Skamarock, W. C., and Coauthors, 2008: A description of the Advanced Research WRF version 3. NCAR Tech. Note NCAR/TN–475+STR, 113 pp. [Available online at http://www2.mmm.ucar.edu/wrf/users/docs/arw_v3.pdf.]

Stensrud, D. J., 1996: Importance of low-level jets to climate: A review. *J. Climate*, **9**, 1698–1711, doi:10.1175/1520-0442(1996)009<1698:IOLLJT>2.0.CO;2.

Storm, B., J. Dudhia, S. Basu, A. Swift, and I. Giammanco, 2008: Evaluation of the Weather Research and Forecasting model on forecasting low-level jets: Implications for wind energy. *Wind Energy*, **12**, 81–90, doi:10.1002/we.288.

Sun, S., and G. Zhai, 1980: On the instability of the low level jet and its trigger function for the occurrence of heavy rain-storms (in Chinese). *Sci. Atmos. Sin.*, **4**, 327–337.

——, and D. Lorenzo, 1985: Influence of Tibetan Plateau on low level jet in East Asia. *Sci. Sin.*, **53B**, 68–81.

Tao, S. Y., 1980: *Rainstorms in China* (in Chinese). Science Press, 225 pp.

Taubman, B. F., L. T. Marufu, C. A. Piety, B. G. Doddridge, J. W. Stehr, and R. R. Dickerson, 2004: Airborne characterization of the chemical, optical, and meteorological properties, and origins of a combined ozone-haze episode over the eastern United States. *J. Atmos. Sci.*, **61**, 1781–1793, doi:10.1175/1520-0469(2004)061<1781:ACOTCO>2.0.CO;2.

Thiébaux, J., E. Rogers, W. Wang, and B. Katz, 2003: A new high-resolution blended real-time global sea surface temperature analysis. *Bull. Amer. Meteor. Soc.*, **84**, 645–656, doi:10.1175/BAMS-84-5-645.

Van de Wiel, B. J., A. Moene, G. Steeneveld, P. Baas, F. Bosveld, and A. Holtslag, 2010: A conceptual view on inertial oscillations and nocturnal low-level jets. *J. Atmos. Sci.*, **67**, 2679–2689, doi:10.1175/2010JAS3289.1.

Wang, Z., K. Gao, and G. Zhai, 2003: A mesoscale numerical simulation of low level jet related with the southwest vortex (in Chinese). *Chin. J. Atmos. Sci.*, **27**, 75–85.

Weaver, S. J., and S. Nigam, 2008: Variability of the Great Plains low-level jet: Large-scale circulation context and hydroclimate impacts. *J. Climate*, **21**, 1532–1551, doi:10.1175/2007JCLI1586.1.

Yu, R., T. Zhou, A. Xiong, Y. Zhu, and J. Li, 2007: Diurnal variations of summer precipitation over contiguous China. *Geophys. Res. Lett.*, **34**, L01704, doi:10.1029/2006GL028129.

Zhang, D.-L., and J. M. Fritsch, 1986: Numerical simulation of the meso-β scale structure and evolution of the 1977 Johnstown flood. Part I: Model description and verification. *J. Atmos. Sci.*, **43**, 1913–1943, doi:10.1175/1520-0469(1986)043<1913:NSOTMS>2.0.CO;2.

——, S. Zhang, and S. J. Weaver, 2006: Low-level jets over the mid-Atlantic states: Warm-season climatology and a case study. *J. Appl. Meteor.*, **45**, 194–209, doi:10.1175/JAM2313.1.

Zhao, P., and X. Zhou, 2001: Formation of low-level meso-scale southwest jet during seasonal rainfall. *Prog. Nat. Sci.*, **11**, 272–279.

Zhao, Y., 2012: Numerical investigation of a localized extremely heavy rainfall event in complex topographic area during midsummer. *Atmos. Res.*, **113**, 22–39, doi:10.1016/j.atmosres.2012.04.018.